Research article

Design of battery shell stamping parameters for vehicles based on fusion of various artificial neural network models

Na Liu [*], Yuanyuan Gao, Peng Liu

School of Mechanical and Electrical Engineering, Shandong Jianzhu University, Jinan, 250101, China

ABSTRACT

The application of neural network model in engineering prediction is frequent. The BPE shell material was optimized, and the reliability of the new material was verified by modal simulation. The accuracy of finite element modeling was ensured by constrained mode experiments, and all variables were preprocessed by Latin hypercube sampling. The design parameters were determined by Monte Carlo simulation. Four different neural networks, including back propagation (BP), radial basis function (RBF), extreme learning machine (ELM) and wavelet neural network (WNN), are used to train and learn the dataset. The BPE weight reduction ratio was 14.3%, the stress was reduced by 18.6%, deformation displacement was reduced by 14.2%, and the first-order mode was increased by 29.1%.

1. Introduction

With the gradual reduction of the earth's primary energy sources, the focus of research in many countries has changed to the storage of secondary energy (electricity and heat) [1]. The lightweight of the entire vehicle is one of the most feasible and economical solutions to reduce the environmental impact of the typical vehicle life cycle operation phase [2]. AkhilGarg et al. summarized an advanced modeling framework for multi-objective optimized design [3]. Liu Fen et al. presented a multi-objective topology optimization design method for traction battery housings [4]. Li Shui et al. used central composite design (CCD), artificial neural network (ANN) algorithms in order to optimize the mechanical design characteristics of the battery pack shell [5]. Xiong and others have developed an effective analysis method for weight reduction and crash resistance of the vehicle battery pack system through orthogonal test design [6,7]. Roland et al. assessed the performance of a mechanical battery pack structure on the basis of energy absorption and packaging efficiency, thus enabling optimization of the EV's overall performance in addition to the actual crash performance [8]. For the lightweight of battery packs, structure, materials are a good way to optimize, in recent years, nanomaterials are widely used in industry [9–13], agriculture and medical treatment, is one of the key means to apply to lightweight in the future. In this paper, finite element analysis (FEA) method is used to establish an accurate finite element model. Because the traditional structural optimization research often only one-sided research and analysis calculation modeling and optimization but did not involve more accurate and efficient optimization design analysis method. In this paper, some improvements are made.

Nomenclature

| Variable	Definition Unit
ω	first-order inherent frequency Hz
ρ	the mass per unit length Kg/m^3
L	length mm
E	modulus of elasticity Dyne per square centimeter
[M]	mass matrix kg
C	damping N·s/m
[K]	stiffness matrix N/m
$\{\ddot{x}(t)\}$	acceleration matrix m/s^2
$\{\dot{x}(t)\}$	speed matrix m/s
$\{x(t)\}$	displacement matrix mm
$\{f(t)\}$	n-order array representing system excitation Hz
t	time variable s
x	the first layer input the number
Z	the first layer output the number
i,j	the neural network node
$W_{i,j^{(1)}}$	the weight between the first nodes 1
$F(a_1^n)$	the output value after the activation function
M	the quality kg
F	frequency Hz

2. BPE finite element analysis

2.1. BPE model simplified

The data parameters of the BPE model studied in this paper come from a pure electric vehicle, and according to the physical material properties of the power pack components [14], the material of the upper cover is changed and upgraded in this paper. The BPE lid is made of sheet molding compound (SMC), which has high strength and high temperature resistance. The material density was reduced from 1800 kg/m^3 to 1670 kg/m^3, the Poisson's ratio changed from 0.26 to 0.35 and modulus of elasticity changed from 8610 MPa to 13 200 MPa. Elastic stiffness is as described in Equation (1) [15].

$$\omega = \frac{\pi}{2L}\sqrt{\frac{E}{\rho}} \tag{1}$$

In expressions, ω-first-order inherent frequency, ρ-the mass per unit length, *L*-length.

If detailed modeling is carried out, it is easy to lead to excessive calculation and increase the calculation cost. However, if the weight of the battery module is replaced by a simple mass point, it will affect the force transmission accuracy between the models. Therefore,
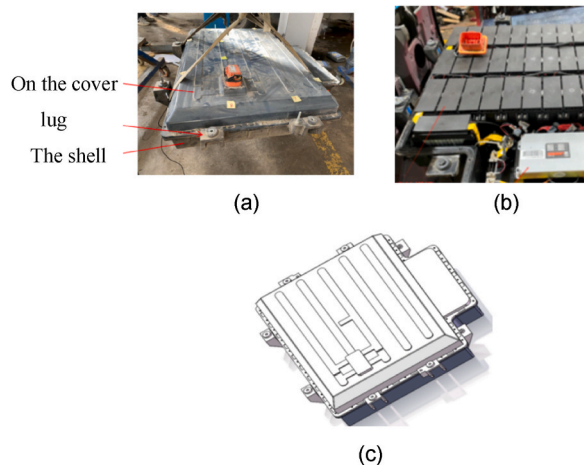
Fig. 1. The BPE simplifies the equivalent model.

in this paper, the battery module is equivalent to a simple geometric entity with equivalent weight [16]. The physical object of the BPE and 3D modeling are shown in Fig. 1. Fig. 1a shows the appearance of the battery, Fig. 1b shows the internal structure of the battery, Fig. 1c shows the implified model for 3D modeling of the battery shell.

2.2. Free modal experiments

During the modal test, the method of multi-point excitation and single-point measurement is used. Sixteen test nodes were selected as excitation input points after establishing an approximate model in the dynamic test system according to the data of the real object and dividing the nodes at each place of length, width and height. Fig. 2 showed the Free modal experimental test rig. Fig. 2a showed the control and display system, 2 b showed the hammer of the test system, 2c showed the constraint form of the model, and 2 d showed overview of the testing instrument.

Post-processing of experimental data: After completing the data acquisition, use the supporting data analysis software to analyze the modal parameters of the collected experimental data based on the frequency response function method, and calculate the frequency response function of the vibration system using dynamic response data of structure obtained from external excitation by using eq. (2) [17].

$$H_{ij}(\omega) = \frac{x_i(\omega)}{f_j(\omega)} = \sum_{r=1}^{m} \frac{\varphi_{ri}\varphi_{rj}}{m_r\left[(\omega_r^2-\omega^2) + j\omega_r c\right]} \tag{2}$$

In the equation: H_{ij}- frequency response function, $x_i(\omega)$ - response of the system, $f_j(\omega)$- modal parameters of the system, m_r- modal mass, φ_{ri} , φ_{rj}- vibration pattern at the excitation point at order r, m - total number of orders of the identified modal parameters, ω^2 - eigenfrequency.

2.3. Comparison of modal simulation and experimental test results

Based on the principle of experimental simulation model error analysis, so the seventh to ninth order mode vibration and frequency are compared with the first to third order results in the experimental model results, as shown in Table 1. The comparison results show that there is a certain error between the finite element results and the experimental results, mainly due to the simplification of the three-dimensional model in the modeling process, resulting in a certain difference between the model and the actual physical parameters of the battery pack. However, the error between the two results is within ±3%, which verifies the correctness of the finite element model.

2.4. Modal analysis theory

According to dynamical system theory, the general equilibrium equation for dynamical systems is as follows in equation (3)-(4) [18]:

$$[M]\{\ddot{x}(t)\} + C\{\dot{x}(t)\} + [K]\{x(t)\} = \{f(t)\} \tag{3}$$

$$[M]\{\ddot{x}(t)\} + [K]\{x(t)\} = 0 \tag{4a}$$

Medium: [M]- mass matrix; C- damping; [K]- stiffness matrix; $\{\ddot{x}(t)\}$- acceleration matrix; $\{\dot{x}(t)\}$- speed matrix; $\{x(t)\}$- displacement
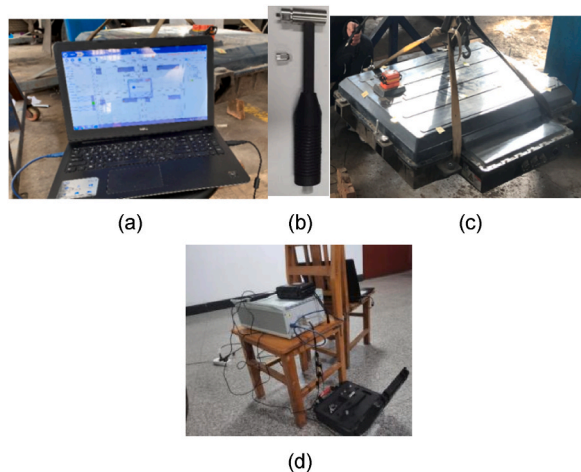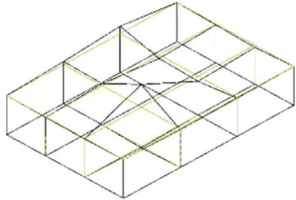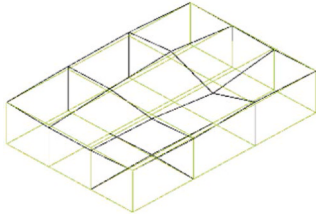

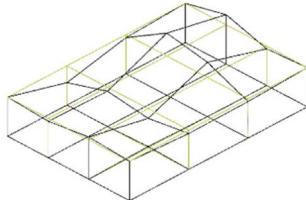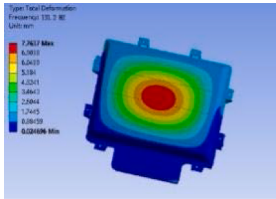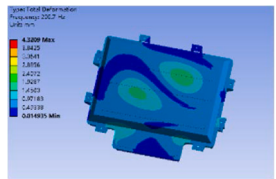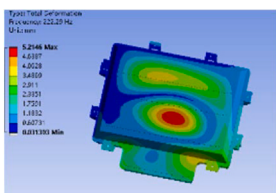
(a)   (b)   (c)

(d)

Fig. 2. Free modal experimental test rig.

Table 1
Comparison of simulation and experimental results.

Experimental results	Experimental results vibration diagram	Experimental modal order (Hz)
First order		128.24
Second order		203.27
Third order		227.97
Simulation results	Simulation calculation vibration pattern diagram	Simulation analysis frequency value (Hz)
Seventh order		131.20
Eighth order		206.70
Ninth order		222.29

matrix; {f(t)}- n-order array representing system excitation; t-time variable.

2.5. Power pack constraint modal analysis

The vibrations and deformations of the BPE were extracted in the modal analysis interface using the modal superposition method of lanczos [19], laying the foundations for analytical calculations below.

3. The construction and training process of the ANN model

First, we need to select the characteristics of the input variables. we simulated the electric vehicle braking and turning under the condition of deformation finite element simulation model for the choice of the characteristics of the input variables, we will be under two different conditions will be BPE all size corresponding to the deformation and stress, as well as the deformation amount of modal deformation in modal analysis, a data set is made, and Monte Carlo simulation technology is used for probability sensitivity analysis to determine input feature vector and reduce later calculation steps.

3.1. Monte Carlo simulation technique probability sensitivity analysis

Multiple indexes are calculated using the Monte Carlo method [20,21], the dimensions of the battery box model are multiple uncertain model inputs $\{T_1, T_2 \dots \}$, and it is also assumed that these design variables all exist uniformly and independently within a hypercube, the battery box model can be regarded as a function $F = f(T)$ of the vibration mode displacement and stress displacement under different working conditions, where T and F are the inputs and outputs of the mathematical model with selected design variables. The specific modeling process is as follows.

When determining sensitivity of each component thickness to the frequency, matrix in above codes:

F = [64.754; 78.794; 72.958; 84.991; 91.704]; Q = [64.754; 78.794; 72.888; 84.999; 81.801]; W = [64.754 64.754 64.754 64.754 64.754 64.754 64.754; 78.794 78.794 78.794 78.794 78.794 78.794 78.794; 72.958 72.958 72.958 72.958 72.958 72.958 72.958; 84.991 84.991 84.991 84.991 84.991 84.991 84.991; 91.675 91.726 81.812 91.704 91.705 91.705 91.696].

Pseudo-code for modeling process

Constructing the ontology matrix, there are three output targets in this paper, namely mass, frequency and stress displacement.
    Set the number of points to be selected for the initialization of the independent variable.
    Upper and lower bounds for independent variables.
    Performing a for loop.
    Split the matrix to generate matrix A, matrix B and matrix A*B.
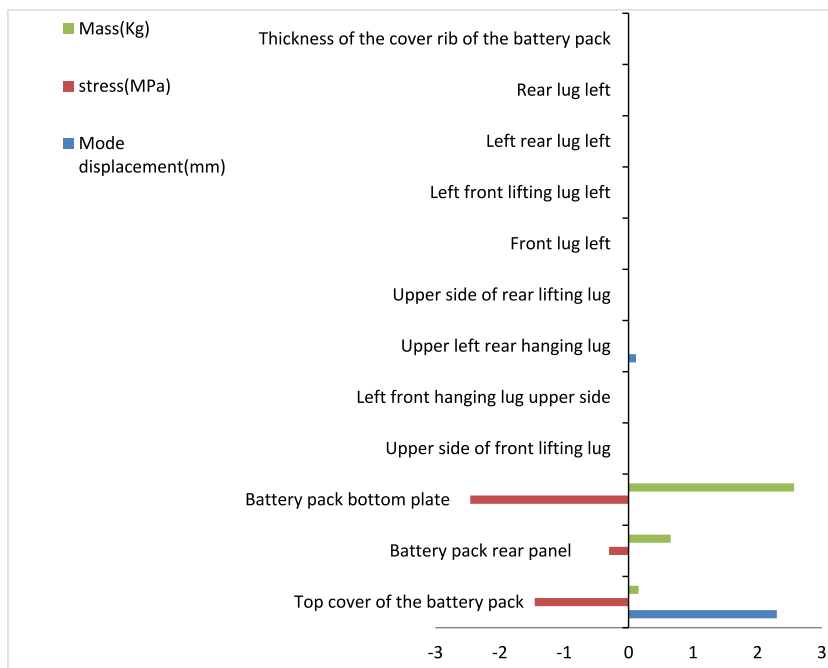
Fig. 3. Sensitivity analysis.

(*continued*)

Pseudo-code for modeling process
Extract the corresponding number of columns or rows of the above generated matrix according to the principles of the algorithm.
Performing a for loop.
Replace column i of matrix A with column i of matrix B.
Corresponding output target matrix:F,Q,W;
F = []', Q = []'; W = []';
Assign row i of F, Q,W to Y(A),Y(B) and Y (AB) respectively;
Use the formula [EX(i) = 1/(2*nPop)* EX(i)+(YA(j)-YAB (j,i))^2,ST(i) = EX(i)+(YA(j)-YAB (j,i))^2/VarY] to

When determining sensitivity of each component thickness to deformation, matrix in the above code:

F = [256.05; 111.38; 149.82; 69.716; 176.92]; Q = [256.05; 111.38; 77.388; 160.13; 131.52]; W = [256.05 256.05 256.05 256.05 256.05 256.05 256.05; 111.38 111.38 111.38 111.38 111.38 111.38 111.38; 149.82 149.82 149.82 149.82 149.82 149.82 149.82; 69.716 69.716 69.716 69.716 69.716 69.716 69.716; 132.96 175.56 176.92 176.92 176.91 176.92 176.92]; When determining the sensitivity of each component thickness to deformation, the matrix in the above code:F = [2.9575; 1.2542; 2.2258; 1.1881; 2.5691]; Q = [2.9575; 1.2542; 1.281; 2.2998; 1.8605]; W = [2.9575 2.9575 2.9575 2.9575 2.9575 2.9575 2.9575; 1.2542 1.2542 1.2542 1.2542 1.2542 1.2542 1.2542; 2.2258 2.2258 2.2258 2.2258 2.2258 2.2258 2.2258; 1.1881 1.1881 1.1881 1.1881 1.1881 1.1881 1.1881; 1.8869 2.5401 2.5692 2.5691 2.5691 2.5691 2.5691]. After the above calculation, the sensitivity values obtained in this paper are drawn into a table, as shown in Fig. 3. The sensitivity of each shift of the battery box to each design feature variable can be clearly and intuitively seen, so as to select the best input feature variable.

Can be seen from Fig. 3, under different conditions, the influence of the BPE shell deformation characteristic variables for the thickness of the BPE shell cover, frame plate and the thickness of the plate after under BPE, BPE four lug the thickness of the upper, so this paper selected the seven features as the input of design variables characteristics.

3.2. ANN model

The ANN model is a computational model based on biological neural networks that mimic the way neurons in the human brain compute and process data. This robust and fault-tolerant model is able to solve tasks where intuition is the only option for humans [22]. Undertake above, this paper respectively in the following chose four different types of neural networks, including the back propagation (BP), radial basis function (RBF) neural network, extreme learning machines (ELM) neural network and wavelet neural network (WNN), to training and testing the model respectively, and the error, training time and so on were analyzed, finally in four different neural networks, The neural network with the best prediction effect is selected to predict and the optimal result is obtained.

3.3. Construction of BP neural network models

At present, the popular neural network model is BP neural network, which is a multi-layer feed forward neural network that uses a back propagation error algorithm for training, verification, and prediction. The number of nodes in the input layer of both ANN models in this paper is 4, and the number of nodes in the output layer is 1. Number of nodes in the hidden layer can be determined by the empirical formula shown in equation (4)-(8) [23].

$$n_h = \sqrt{n_i + n_0} + m, m \in [1, 10] \tag{4b}$$

$$Z_j^n = \sum \left(w_{ji}^{(1)} X^{n-1} i + w_{j0}^{(1)} \right) \tag{5}$$

$$a_1^n = \sum w_{ij}^{(2)} z^{n-1} i + w_{i0}^{(2)} \tag{6}$$

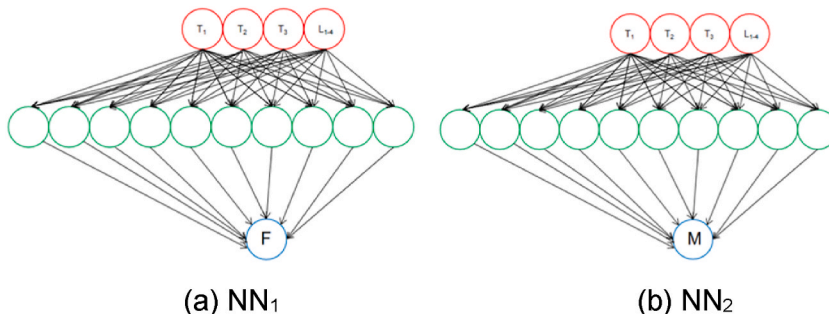(a) NN$_1$ (b) NN$_2$

Fig. 4. The structure of the neural network model.

$$a = f(W_P + B) \tag{7}$$

$$y_1^n = F(a_1^n) \tag{8}$$

Eight hidden layer nodes are used in paper. These parameters are distributed to next layer, with data distribution computation rules as in eqs. (5)–(8).

In the formula, x represents the first layer input, z represents the first layer output, i represents the neural network node, $W_{ji}^{(1)}$ represents the weight between the first nodes, $F(a_1^n)$ represents the output value after activation function, represents the weight deviation between w neurons.

BP neural network combined with gradient descent algorithm calculation principle and design variables to build the corresponding neural network model as shown in Fig. 4. NN$_1$(Neural network model 1) referred to the target results of the BPE first order frequency F. NN$_2$(Neural network model 2) referred to the target results of the BPE weight M. The NN$_1$ and NN$_2$ mentioned in the following paper were explained the same as here.

Then according to the ANN model of the design variables after random combination, the target results of the BPE first order frequency F and weight M, a total of 60 sets of sample data selected as Table 2.

As existing structural lightweight designs focus on dimensional changes or material variations of components that affect the fatigue life of the BPE, the factors that make up the BPE housing are used as design variables [24]. The main factors affecting the weight and inherent frequency of the BPE were selected as design variables: the thickness of the upper and lower BPE shells, the thickness of the upper BPE shell and other dimensions, as shown in Fig. 5.

Due to manufacturing conditions, the thickness of the upper guest body, which has a large influence on the BPE frequency, should be greater than 2 mm. In addition, a range of common dimensions for manufacturing BPE housings was combined (Table 2). A random combination of design variables was designed, then 60 sets of data were selected, and the corresponding combined structural masses and first order frequencies were calculated as shown in Figs. 6–9. 1–15 Group Output Variable Quality and Frequency Value were shown in Fig. 6 [15],-29 were shown in Figs. 7, 30–44 were shown in Figs. 8, 45–60 were shown in Fig. 9.

Due to the large data fluctuations in this paper, in order to ensure the reliability and improve the training results and learning efficiency, the data is first reprocessed, namely, using the map minmax (.) function in MATLAB·, so that the data can fluctuate stable in the range of 0–1.

After the ANN model has been trained on the sample data, the accuracy of the model needs to be tested in this paper. The neural network model is trained and processed according to the model structure, input model parameters and number of nodes designed in this paper, and the prediction structure is evaluated by continuously changing the size of the weights, and finally the accuracy of both training and prediction results are evaluated using mean absolute error, calculated as in eq. (9) [18].

$$e_{avg} = \frac{1}{n} \sum_{k=1}^{n} \left| \text{Output}_k \text{-Output}_{r,k} \right| \tag{9}$$

In the formula: e_{avg} represents the average absolute error. N represents the number of data points. Output $_k$ represents the k th estimated output parameter. Output $_{r, k}$ represents the k th reference estimated output parameter. After the training parameters of the above models were set, the training process of the two neural network regression models is shown in Fig. 10., they both achieved ideal error convergence rate after initialization.

The NN1 model was terminated after 24 iterations of the sample data, and the generalization of the ANN model shows that if the mean square error (MSE) does not fall but rises for 6 consecutive times during the training process, the network stops training, and it can be seen that the training is terminated when the gradient value is 14.6765 and no longer falls for 6 consecutive times, and the NN1 model is terminated. For the NN2 model, after 22 iterations of the data, the gradient value was 2.9561 and the training was terminated when it stopped falling for 6 consecutive times, and the NN2 model terminated the iterative training. As seen from Fig. 10, the NN2 model has fewer iterations, less usage, and a lower gradient at iteration termination. The regression performance pair of N1 and N2 is shown as shown in Fig. 11. From the results of the model training, Fig. 11 shows the degree of fit between the network output value and the actual value. The larger the r value, the better the network training. Therefore, from the comparison between NN1 and NN2, the training effect of NN2 is better than NN1, and the overall training effect of NN2 is better.

The model is trained to have a higher fit accuracy, as shown in Table 3.

The training result curves of the two neural network regression models are shown in Fig. 12. It can be intuitively seen from the two curves that the training set, the test set and the validation set all regress close to the optimal values, which means that the training effect is good as well as the representativeness of the data and the reliability of the model.

According to the graph of the model training, the NN1 model was trained best to the 18th generation, and the NN2 model was trained best to the 16th generation.

Table 2
Designs the range of variable values.

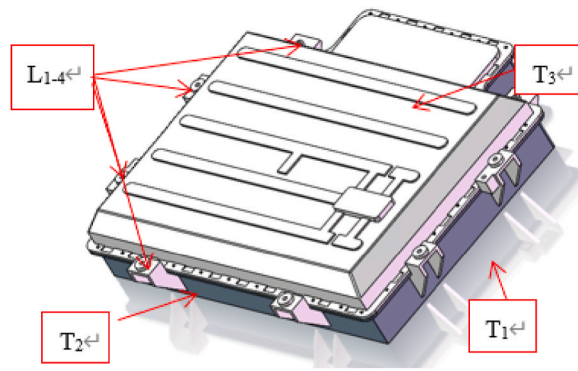| Name of the variable	Thickness of bottom shell T1 (mm)	Thickness of rear side plate T2 (mm)	Cover thickness T3 (mm)	Hanging ear (1–4)thickness L1~L4 (mm)
Data	1–5	1–4	3–5	7–9

Fig. 5. Design variable corresponding position.
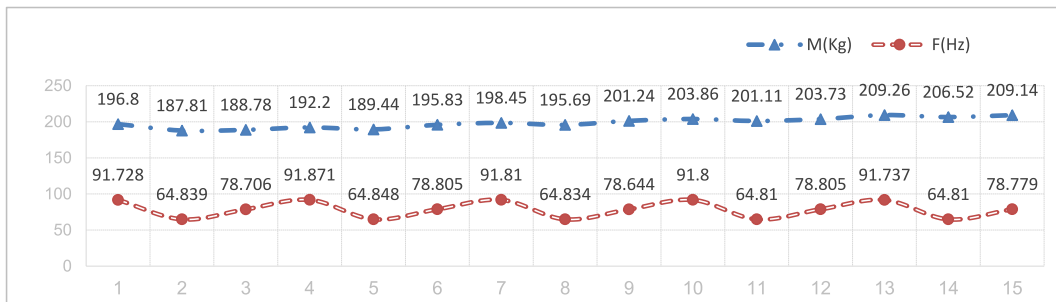

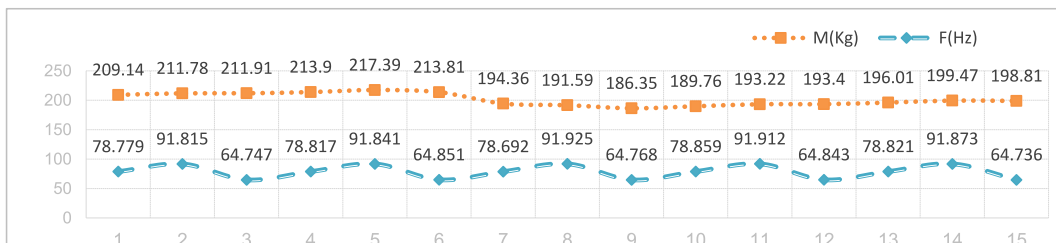**Fig. 6.** 1–15 group output variable quality and frequency value.

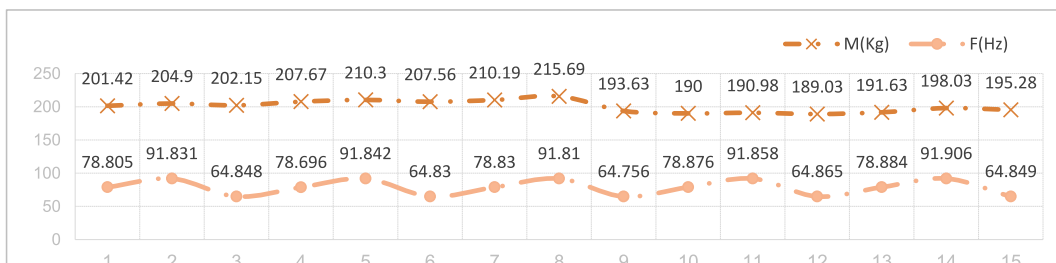**Fig. 7.** 15–29 group output variable quality and frequency value.

Fig. 8. 30–44 group output variable quality and frequency value.

The histogram of the variance distribution of the two neural network regression models is shown in Fig. 13. The general direction of this error distribution result curve is in accordance with the Gaussian distribution rule, i.e. normal distribution [25], and it can be seen from the data that the errors are mainly concentrated around ±0.9, indicating the representativeness of the training data and the reliability of the model. From the results of model training, to test the training effect of the network, the better the training effect, NN1 and NN2 are close to the normal distribution, and NN2 model error distribution than NN1, error distribution is more concentrated, and
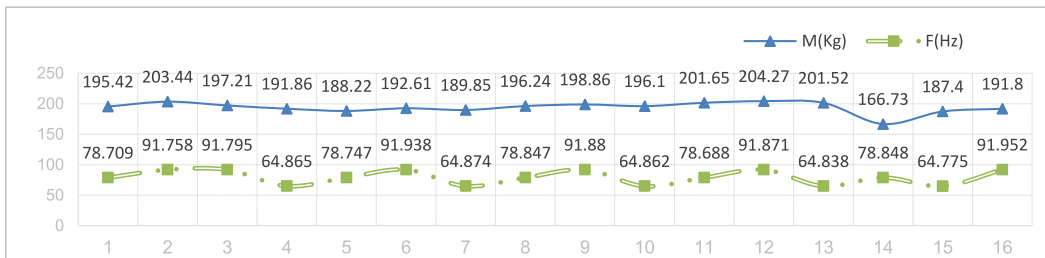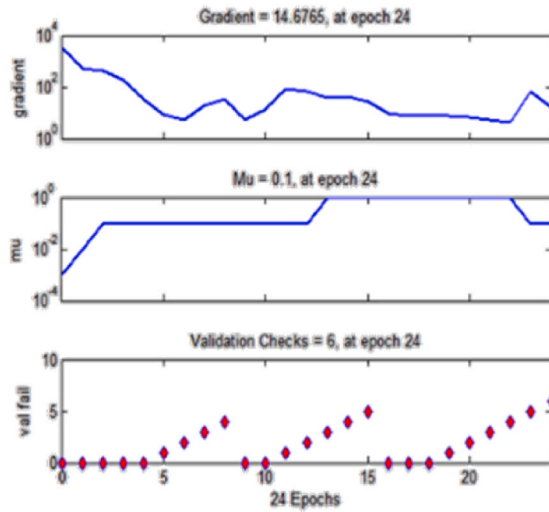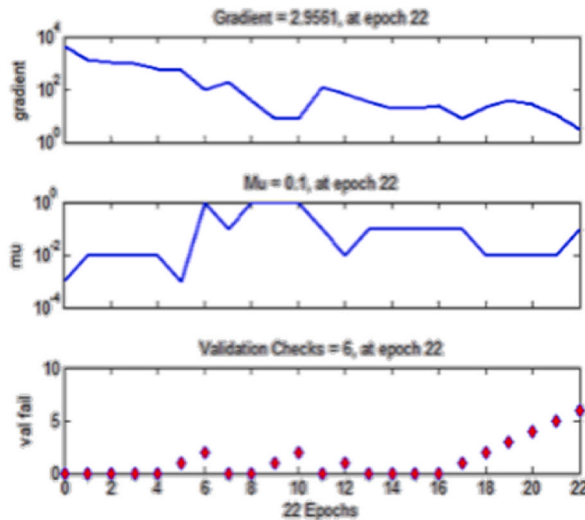
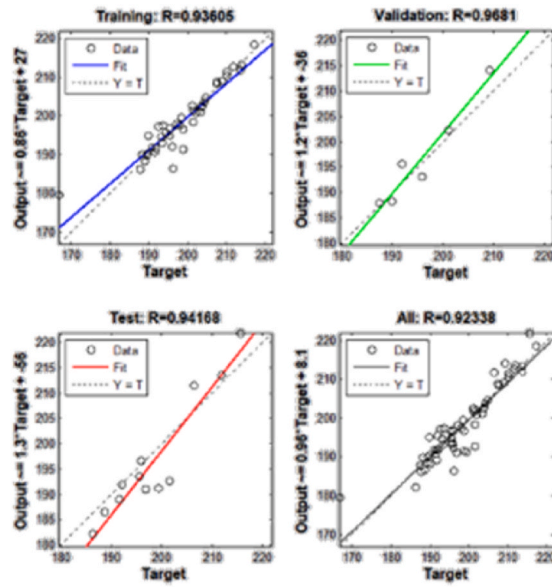**Fig. 9.** 45–60 sets of output variable quality and frequency values.
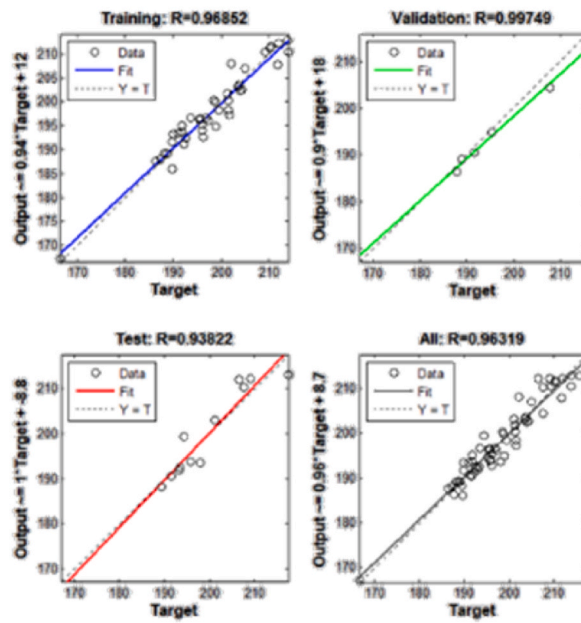

(a) NN$_1$

(b) NN$_2$

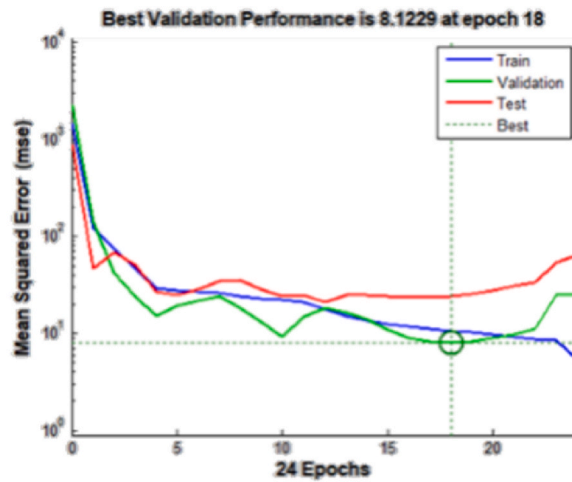**Fig. 10.** Neural network model regression curve.

(a) NN₁

(b) NN₂

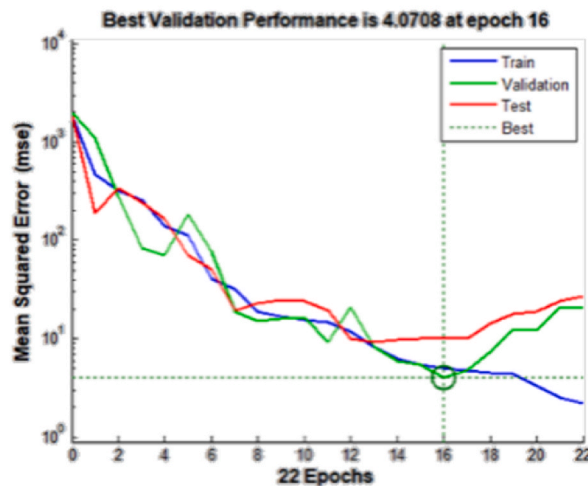**Fig. 11.** Regression performance analysis curve.

Table 3
The results of the training fit of the nerve model sample data.

| Fit accuracy model	Training (%).	Verify (%).	Test (%).	Overall (%).
NN1	93.606	96.810	94.168	92.338
NN2	96.862	99.749	93.822	96.319

(a) NN$_1$

(b) NN$_2$

Fig. 12. Regression performance analysis curve.

closer to the positive distribution, NN2 model error is concentrated and force close to zero error, with better training effect. From overall training results are available, the NN2 model training effect is slightly better than NN1 model, so choice of data group is reasonable.
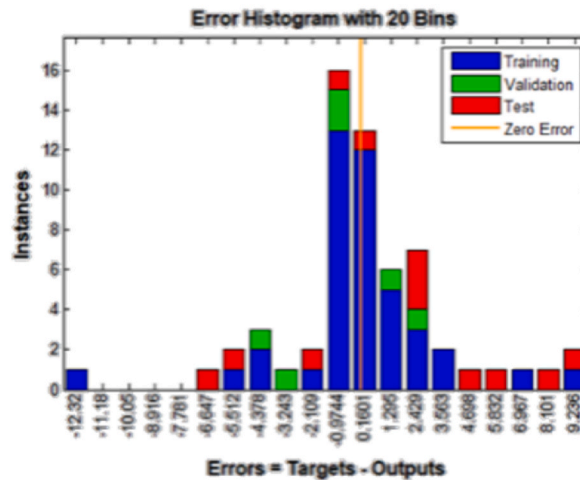
3.4. Construction of RBF neural network models

The topology of radial basis neural network [26] is similar to BP, though with a three-layer forward network. Different from the BP neural network described above, the BP neural network is a global approximation for nonlinear mapping, using the sigmoid function as an activation function, while the radial-based neural network is a local approximation for nonlinear mapping, using the Gaussian function as a kernel function. The selection of the data set is not described above. After a series of training calculations, the training test results are shown in Fig. 14.

As can be seen from the training results, by randomly dividing the test set, after multiple training, the best test set accuracy of NN1 model is only 79.714%, the effect is poor, and the accuracy of NN2 model can reach 92.445%.
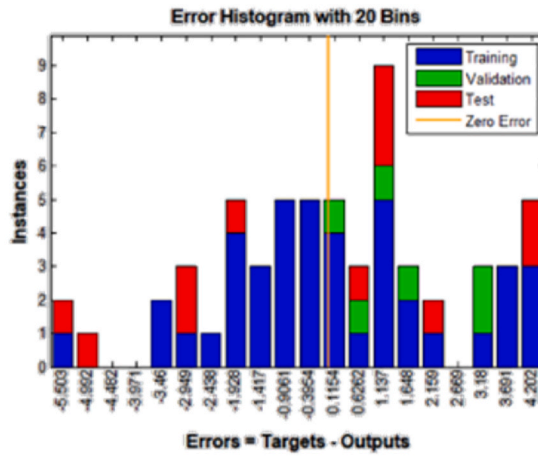
(a) NN$_1$

(b) NN$_2$

Fig. 13. The error distribution histogram.

3.5. Construction of ELM neural network models

The topology of the extreme learning machines network is different from that mentioned above, and features nodes hidden by random output. When adjusting the weights, without back propagation through a gradient such as the BP neural network, it only takes one step to train the output weight, that is, the weights are set through Moore Penrose generalized inverse [27]. Computational accuracy varies across data groups and can be used in scenarios requiring immediate computation. The training results are shown in Fig. 15.

From the training results, through random division of the test set, the best test set accuracy of the NN1 model is only 80.942%, and the effect is poor. The test error fluctuates between-20 and 10; the NN2 model can reach 99.987%, and the test error only fluctuates between −0.1 and 0.2.

3.6. Construction of WNN neural network models

The topology of the wavelet neural network is roughly similar to the traditional neural network, but by changing the function at the hidden layer node to the wavelet basis function to transmit when the signal is transmitted from input to output, the error is back propagated, then adjust the weights and bias between the input layer and the hidden layer, as well as the weights and bias between the
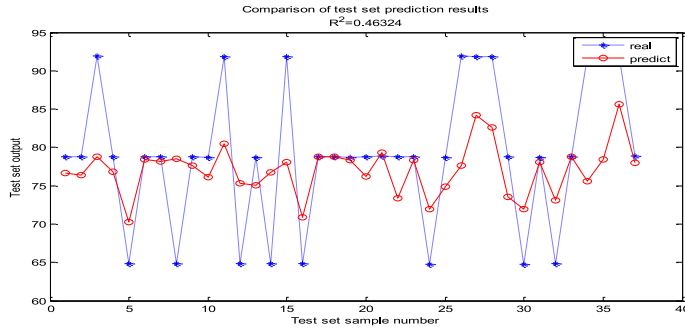
(a) NN$_1$

(b) NN$_2$

Fig. 14. RBF: Comparison of test set prediction results.

implied layer and the output layer. When constructing the training sample, the paper is different from previous fixed inputs, the input data set is ran perm selected using the rand perm function, and the resulting training structure is shown in Fig. 16.
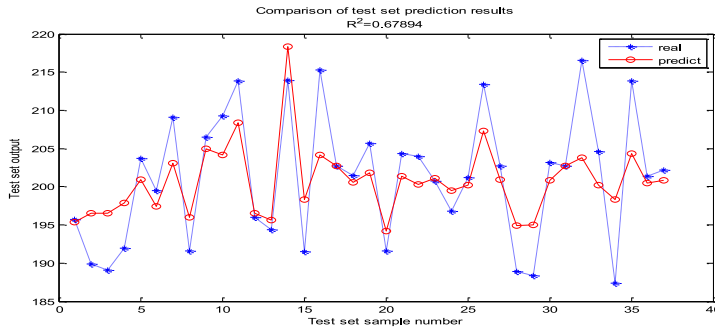
From the training results, through the random division of the test set, the best test set accuracy of the NN1 model was only 74.187%, with a poor effect. The test error curve fluctuates greatly; the prediction accuracy of the NN2 model can only reach 80.48%, and test error also has a poor effect.

3.7. Comparison of the results of the four neural networks

By constructing the four different neural network models described above, and the inputs and outputs we need training, the test result pairs are shown in Table 4.

We can see that although the extreme learning machines neural network trains fast, the NN1 model has never achieved satisfactory test results, and the radial basis network and WNN network have unsatisfactory test effect and large error. In conclusion, the BP neural network is selected as the most suitable test model and makes data prediction.

4 Best Results Prediction

In this paper, the seven factors affecting the thickness of the BPE are randomly combined in steps of 0.5 m using the ndgrid function in MATLAB.

After the combination, 196 875 sets of predicted data were finally obtained. Using the above procedure, the ANN model was applied to the 196 875 sets of randomly combined data to predict the mass and first-order frequency. The selection criteria for the final optimization scheme are as follows.

$$\begin{cases} \min M = \sum_{i=1}^{n} M_i \ (n = 1, 2, 3, \ldots, 8) \\ \min F \geq 70 \ \text{Hz} \\ T_i^{\min} \leq T_i \leq T_i^{\max} \ (i = 1, 2, 3) \\ L_j^{\min} \leq L_j \leq L_j^{\max} \ (j = 1, 2, 3, 4) \end{cases} \tag{10}$$

Optimization scheme for group 2872 is finally selected from 196 875 sets of data, as shown in Table 5.

In accordance with the above criteria for the selection of design variables and target quantities, the prediction results of each part
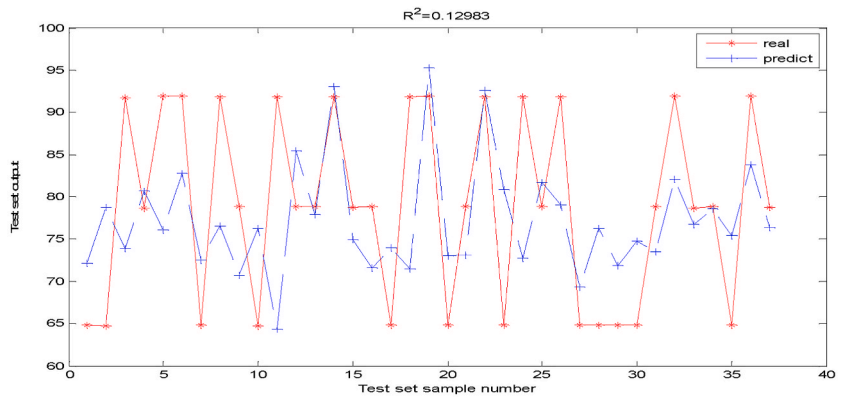
(a) NN$_1$
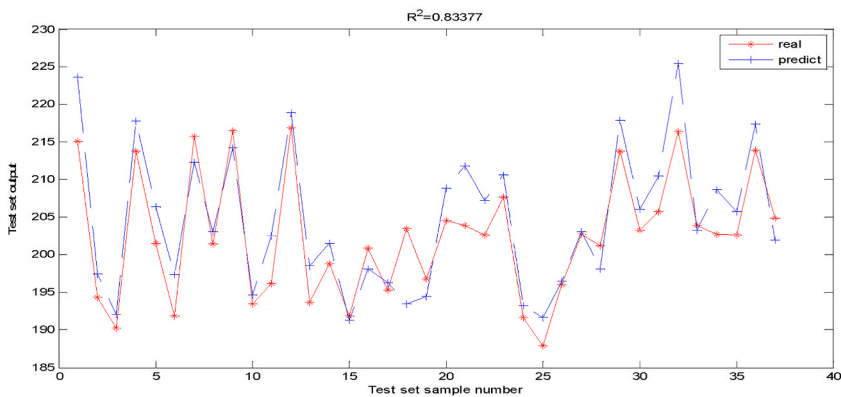
(b) NN$_2$

Fig. 15. ELM: Comparison of test set prediction results.

were modeled and analyzed, and the comparative quality and first-order frequency results were calculated by finite element software analysis as shown in Table 6, the error between the optimization scheme and the simulation results were within ±4%, in line with the theoretical calculation requirements, i.e. Optimized prediction scheme has certain reliability.

## 4. Static mechanics analysis of the optimized BPE structure

As the impact of bumpy roads on the BPE is large, to ensure the reliability of the optimized solution, this paper selects the combined working conditions under bumpy roads and sharp turns for the static analysis of the BPE. The maximum forces under the driving conditions of the electric vehicle are solved and analyzed separately, with grid orthogonal mass ratio of 0.85. The g is the free fall acceleration, g = 9.8 m/s^2. When the electric vehicle makes a sharp turn at 80 km/h on a bumpy road, there is lateral acceleration and vertical inertial acceleration of the BPE as a whole. The optimized stress and displacement distribution of the BPE structure under this condition is shown in Fig. 17 (the unit of stress in the figure is MPa and the unit of displacement is mm).

As can be seen from Fig. 17a, the maximum stress in the original model BPE structure under sharp turning conditions on bumpy roads is 185.27 MPa, which is located at the left front side of the BPE bottom shell, which is less than the yield strength of dc01 material of 210 MPa. As can be seen from Fig. 17b, the most serious deformation area is 2.1789 mm on the left side of the lower shell, which meets the requirements of the material. As can be seen from the diagram, the first-order intrinsic frequency is 130.68 Hz and the maximum deformation is 13.767 mm, which occurs in the middle of the upper cover, achieving the purpose of optimization. The above neural network prediction results show that although reducing the wall thickness of each component can reduce the mass, it can easily lead to excessive stress or stress concentration. Therefore, in the following, the paper had added cross-shaped thin-walled reinforcements to target the stress weaknesses to improve the stiffness of the battery shell while reducing mass. The resulting stress results and stress displacements are shown in Fig. 18.

From the FEA results, as can be seen from Fig. 18a, the stress magnitude of the optimized BPE model is 156.67 MPa. As can be seen from Fig. 18b, the stress displacement is 1.9016 mm under the same working conditions, which are both significantly lower than before the optimization, proving that the model is better optimized. Fig. 18c shows the 3D model of the battery shell used for analysis.
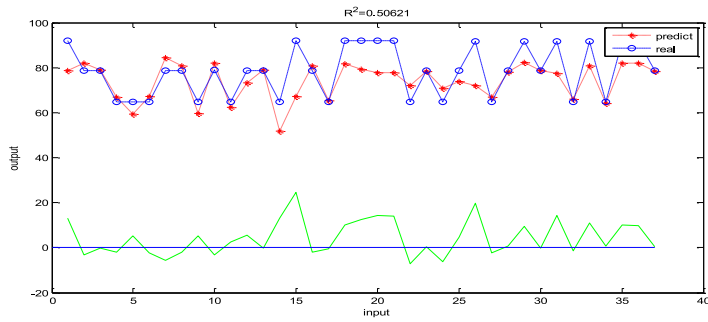
(a) NN₁
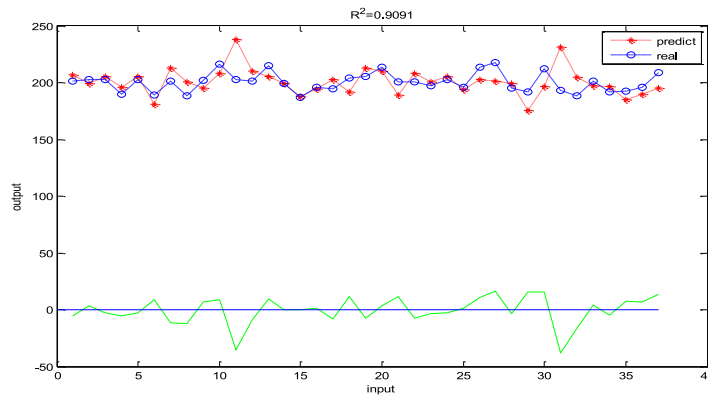
(b) NN₂

Fig. 16. WNN: Comparison of test set prediction results.

Table 4
The resulting contrast.

Neural network type	BP	RBF	ELM	WNN
NN1 Test set accuracy (%)	94.168	46.324	12.983	50.621
NN2 Test set accuracy (%)	93.822	67.894	83.337	90.91

Table 5
The neural model predicts optimal results.

	T1 (mm)	T2 (mm)	T3 (mm)	L1 (mm)	L2 (mm)	L3 (mm)	L4 (mm)	M (kg)	F (Hz)
Best result	1	1	5	8	9	9	7.5	187.93	88.83

Table 6
Optimizes results validation.

Output	M(kg)	F(Hz)
Predict the result	187.9332	88.8359
Simulation validation	190.84	91.826
Error (%).	−1.54	−3.2

5. Conclusion

In this paper, the finite element constrained mode method is used to verify the accuracy of the constructed model and the application of boundary conditions by the error of experiment and simulation not exceeding ±3%, which lays a foundation for the
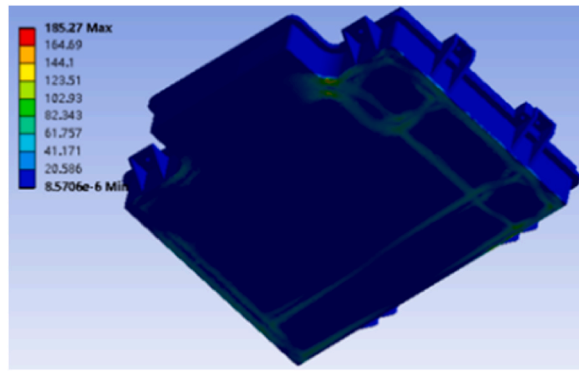
(a) Model Stress Cloud Map
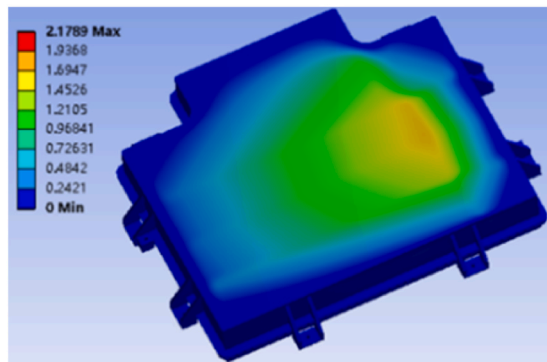
(b) Model Displacement Cloud Map

Fig. 17. Stress and displacement cloud diagram during rough road turning conditions.

optimization of the battery pack model later.

In this paper, static analysis is used to verify the values of battery pack stress and strain under various complex working conditions, and the before and after optimization is compared to see the reliability of optimization. In this paper, the method of constructing the ANN model is adopted, and all variables are preprocessed by Latin hypercube sampling. Monte Carlo simulation determines the required machining design parameters.

In this paper, four different neural networks, including backpropagation (BP), radial basis functions (RBF), extreme learning machines (ELM), and wavelet neural networks (WNN), were used and compared with the training and learning datasets to find the model with the best prediction with a fitting rate of more than 92%. Tens of thousands of sets of data are composed of a certain step size for the design parameters, and the neural network model is used to make regression prediction, so that a set of data with low quality and high frequency is found according to the set constraints.

In this paper, the dimensional optimization design of material change and shell thickness of a vehicle power pack structure is optimized, and the static mechanical analysis of the optimized BPE is carried out. Finally, the weight reduction ratio of BPE was reduced by 14.3%, the stress was reduced by 18.6%, the deformation displacement was reduced by 14.2%, and the first-order mode was increased by 29.1%.

Prospect

This paper mainly uses BP neural network to regression prediction of battery pack processing parameters, but there is still room for optimization in prediction accuracy, and in the future, bionic algorithms can be used to optimize the initial weight and threshold of the neural network to improve the accuracy of prediction, so as to optimize the battery pack processing parameters.

In terms of structural optimization, topology optimization and biomimetic optimization can be used to strengthen its stress concentration and weak points, and in terms of materials, lighter and tougher materials can be used. Examples include nanoscale materials or more novel materials.

The optimized battery pack can be further verified experimentally.

(a) Model Stress Cloud Map

(b) Displacement Cloud Map

(c) The 3D model
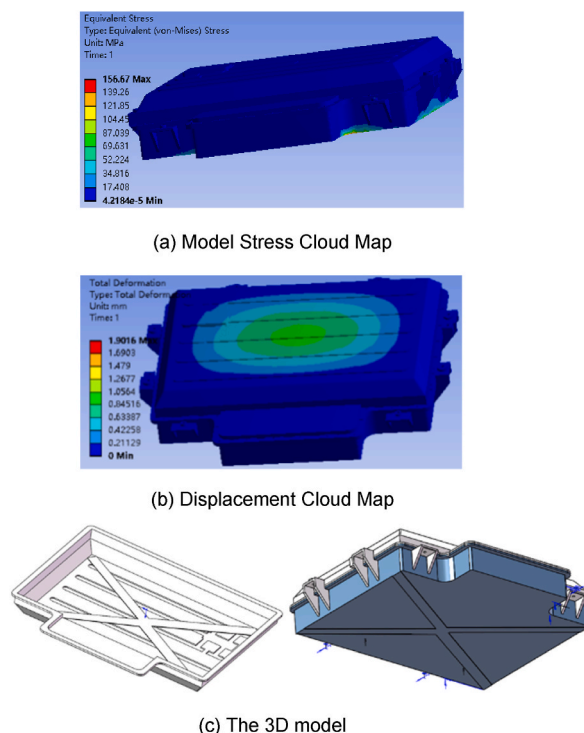
Fig. 18. Finite element analysis results after optimization.

Data availability statement

The data used to backing the findings of the study are available within the article.

Additional information

No additional information is available for this paper.

CRediT authorship contribution statement

Na Liu: Writing – review & editing, Supervision, Resources, Project administration, Methodology, Investigation, Formal analysis, Data curation, Conceptualization. **Yuanyuan Gao:** Writing – original draft, Methodology, Investigation, Formal analysis, Data curation, Conceptualization. **Peng Liu:** Resources, Methodology.

Declaration of competing interest

The authors declare that they have no known competing financial interests or personal relationships that could have appeared to influence the work reported in this paper.

References

[1] Aneke, Mathew1;Wang, & Meihong1(Meihong.Wang@hull.ac.uk), Energy storage technologies and real life applications – a state of the art review, Appl. Energy 179 (0) (2016) 350–377.
[2] Mayyas Ahmad, Mohammed Omar, Mohammed Hayajneh, Raouf Mayyas Abdel, Vehicle's lightweight design vs. electrification from life cycle assessment perspective, J. Clean. Prod. 2017 (2017), https://doi.org/10.1016/j.jclepro.2017.08.145.
[3] Akhil Garg, Xiongbin Peng, My Loan Phung Le, C.M.M. Chin, Design and analysis of capacity models for Lithium-ion battery, Measurement 2018 (2018), https://doi.org/10.1016/j.measurement.2018.02.003.
[4] Fen Liu, Jianfeng Wang, Yiqun Liu, Fuqiang Wang, Na Yang, Xiaodong Liu, Bo Huang, Performance analysis of phase change material in battery thermal management with biomimetichoneycomb fin, Appl. Therm. Eng. 2021 (2021), https://doi.org/10.1016/J.APPLTHERMALENG.2021.117296.
[5] Shui Li, Fangyuan Che, Akhil Garg, Jian Zhang, Design optimization of battery pack enclosure for electric vehicle, Struct. Multidiscip. Optim. 1 (2018), https://doi.org/10.1007/s00158-018-1901-y.
[6] Mossali Elena, Gentilini Luca, Merati Giulia, Colledani Marcello, Methodology and Application of Electric Vehicles BPEs Redesign for Circular Economy, Procedia CIRP, 2020, https://doi.org/10.1016/J.PROCIR.2020.01.139.

[7] Xiong Yue, Yongjun Pan, Lei Wu, Binghe Liu, Effective weight-reduction- and crashworthiness-analysis of a vehicle's battery-pack system via orthogonal experimental design and response surface methodology, Eng. Fail. Anal. 128 (2021) 105635, https://doi.org/10.1016/j.engfailanal.2021.105635. ISSN 1350-6307.

[8] Uerlich Roland, Karthik Ambikakumari Sanalkumar, Tjorben Bokelmann, Thomas Vietor, Finite element analysis considering packaging efficiency of innovative battery pack designs, Int. J. Crashworthiness 25 (6) (2020) 664–679, https://doi.org/10.1080/13588265.2019.1632545.

[9] M. Abdul Basit, M. Imran, S.A. Khan, et al., Partial differential equations modeling of bio-convective sutterby nanofluid flow through paraboloid surface, Sci. Rep. 13 (1) (2023) 6152.

[10] M.A. Basit, U. Farooq, M. Imran, et al., Comprehensive investigations of (Au-Ag/Blood and Cu-Fe3O4/Blood) hybrid nanofluid over two rotating disks: numerical and computational approach, Alex. Eng. J. 72 (2023) 19–36.

[11] M.A. Basit, M. Tahir, A. Riasat, et al., Numerical simulation of bioconvective Casson nanofluid through an exponentially permeable stretching surface, Int. J. Mod. Phys. B (2023) 2450128.

[12] M. Tahir, A. Naz, M. Imran, et al., Activation energy impact on unsteady Bio-convection nanomaterial flow over porous surface, AIMS Mathematics 7 (11) (2022) 19822–19845.

[13] M. Imran, S. Yasmin, H. Waqas, et al., Computational analysis of nanoparticle shapes on hybrid nanofluid flow due to flat horizontal plate via solar collector, J. Nanomater. 12 (4) (2022) 663.

[14] Nannan Liu, Jijun Shi, Changjiang Song, Application and research on the upper shell of battery pack based on OptiStruct composite material, Automotive Technology & Material (8) (2019) 15–20.

[15] K.J. Niklas, F.C. Moon, Flexural stiffness and modulus of elasticity of flower stalks from Allium sativum as measured by multiple resonance frequency spectra, Am. J. Bot. 75 (10) (1988) 1517–1525.

[16] Wei Ouyang, Optimization Design and Safety Study of Automobile Power Battery Pack [D], Nanchang University, Nanchang, 2019.

[17] Zhonggang DU, Yonghou Sun, Fuyun Liu, et al., Improved method of inertial parameter identification based on frequency response function, Instrumentation Technology and Sensors 477 (10) (2022) 116–122.

[18] Changqing Cui, Structural Analysis and Optimization Design of Vehicle Power Battery pack[D], Shandong Jianzhu University, 2021, https://doi.org/10.27273/d.cnki.gsajc.2021.000556.

[19] Seongsoo Lee, Hyungsoo Mok, Chang-Wan Kim, On a component mode synthesis on multi-level and its application to dynamics analysis of vehicle system supported with spring-stiffness damper system[M], J. Mech. Sci. Technol. (12) (2011), https://doi.org/10.1007/s12206-011-1219-9.

[20] B.A. Kaixian, et al., Mass modeling and sensitivity analysis of lightweight hydraulic actuator for legged robot, J. Mech. Eng. 2021 (2021), https://doi.org/10.3901/JME.2021.24.039.

[21] Longli, Shansuo Zheng, Yan Zhou, et al., Parallel Study of Seismic Reliability Analysis of Water Supply Pipe Network Based on Quasi-Monte Carlo Method [J], Journal of Zhejiang University (Engineering edition, 2020, p. 2020, 10.3785/j.issn.1008-973X.2020.02.

[22] S. Parwaiz, O.A. Malik, D. Pradhan, M.M. Khan, Machine-learning-based cyclic voltammetry behavior model for supercapacitance of Co-doped ceria/rGO nanocomposite, J. Chem. Inf. Model. 58 (12) (2018) 2517–2527, https://doi.org/10.1021/acs.jcim.8b00612.

[23] Lei Yang, Study of GNSS R cropland soil moisture retrieval method, Acta Greodaetica et Cartographica Sinica 47 (2017).

[24] Youngsuk Jung, Sunghoon Lim, Jongmin Kim, Seungjae Min, Lightweight design of electric bus roof structure using multi-material topology optimisation, Struct. Multidiscip. Optim. (3) (2020), https://doi.org/10.1007/s00158-019-02410-8.

[25] S.R. Arridge, P. van der Zee, M. Cope, D. Delpy, T.,Reconstruction methods for infrared absorption imaging Proc. SPIE 204 (1991) 1431.

[26] Anqi Chen, D. Airey Gordon, Thom Nick, Litherland Jack, Adjetey Nii-Adjei Rufus, Modelling the stiffness development in asphalt concrete to obtain fatigue failure criteria, Construct. Build. Mater. 2021 (2021), https://doi.org/10.1016/J.CONBUILDMAT.2021.124837.

[27] Katsuaki Tanabe, Pareto's 80/20 rule and the Gaussian distribution, Phys. Stat. Mech. Appl. 2018 (2018), https://doi.org/10.1016/j.physa.2018.07.023.